Three-Dimensional Entanglement: Knots, Knits and Nets

Myfanwy Ella Evans

January 2011

A thesis submitted for the degree of Doctor of Philosophy
of The Australian National University

Department of Applied Mathematics
Australian National University

Chapter 5

Dilatancy of Woven Filament Arrays

We have developed a technique to generate a variety of close-packed arrays of one dimensional filaments, *via* projection of free tilings in the two-dimensional Hyperbolic plane ($\mathbb{H}^2$) into three-dimensional Euclidean space ($\mathbb{E}^3$), as decribed in Ch. 3. A rich catalogue of filament are constructed using this technique, with varying degrees of entanglement of the filaments. In Ch. 4, we have adapted algorithms developed to form canonical 'ideal' or 'tight' embeddings of knots [Katr 96, Pier 98] to arrive at canonical geometries for our weavings.

The existence of curvilinear filament geometries in tight weavings has an unexpected consequence, namely the possibility of 3D weavings that exhibit *dilatancy*, accompanied by a lowering of the fibre packing fraction and the formation of a more open weave: the volume of the weaving may be expanded while maintaining the inter-filament contacts through filament straightening. Equivalently, an internally driven straightening of the filaments within the tight configuration of a dilatant weaving will result in an expansion of the material without loss of filament contacts. We see dilatancy as an attractive material property and dilatant weaving as design target for new materials.

The free volume within a chiral, cubic and finitely dilatant weaving, the ideal conformation of the G_{129C} structure, a helical version of the Σ^+ rod packing, expands more than 5-fold on filament straightening. This remarkable three-dimensional weaving allows variation of packing density without loss of structural rigidity and is an attractive design target for materials. We propose that the ideal G_{129C} weaving is formed by keratin fibres in the outermost layer of mammalian skin, likely templated by a folded membrane.

5.1 Dilatant filament weavings

To determine if a 3-periodic weaving is dilatant, end-state configurations of the weaving under dilation must be prescribed. The initial configuration is the ideal form as determined by the **PB-SONO** algorithm described in Ch. 4; this has maximum filament diameter and a maximum number of inter-filament contacts per filament length (standardised by the filament diameter). We call the terminal configuration the *maximal* configuration, realised as follows. The unit cell is repeatedly subjected to homothetic expansion while maintaining the filament diameter, and the filaments subsequently tightened within the swollen unit cell. (This is equivalent to shrinking the filament diameter while maintaining the unit cell size and subsequently tightening the filaments.) The *maximal* configuration is reached when a further unit cell expansion results in a loss of contacts between filaments.

Closer analysis of 3D weavings reveals a rich taxonomy, amongst which we find three distinct classes. The simplest examples exhibit zero dilatancy. In these cases the ideal configuration and the maximal configuration of the weaving coincide. A second class contains weavings which dilate to accommodate a finite change in unit cell volume. When fully dilated, these finitely dilatant weavings retain all inter-fibre contacts and remain jammed. In their least dense state, finitely dilatant weavings contain rectilinear fibres and their fibre packing fraction decreases continuously during dilation, yet remains positive. The third class comprises infinitely dilatant weavings, characterised by a decrease of fibre packing fraction to zero. Since this fully dilated state is only realised for fibres of positive diameter by swelling the unit cell without limit, finite volumes of infinitely dilatant weavings will never realise this limit, since only infinitely long fibres remain jammed. We note that the hypothetical infinitely dilated configuration may consist of straight or curvilinear fibres. (In practice, infinitely dilatant weavings expand until they unjam due to loss of mutual contacts, and this end-state depends on the original fibre length.) Some examples demonstrate these various weaving classes[1].

Numerical tightening of the D_{124C} structure, equivalent to the Π^* rod packing, revealed that the ideal structure is composed of straight rods (Fig. 5.1(a)). Inflation of the unit cell while maintaining the filament diameter induces a reduction in the number of inter-fibre contacts per unit cell (Fig. 5.1(b)). Hence the tight and maximal configurations of this rod packing are equivalent, and we can infer that the weaving is not dilatant.

[1] A further class of finitely dilatant weavings can be imagined for which the maximal configuration contains curvilinear fibres. To date, however, we have failed to find an example of this class.

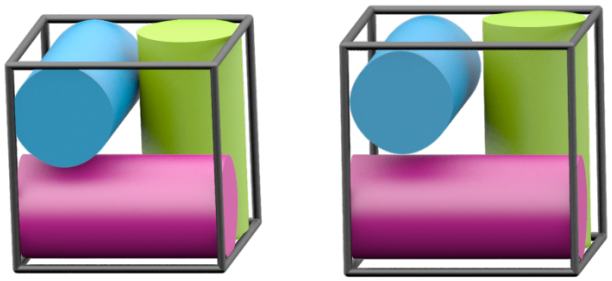

(a) **(b)**

Figure 5.1: The D_{124C} structure, equivalent to the Π^* rod packing, has zero dilatancy. (a) The ideal form of the structure within one unit cell. (b) An expansion of the unit cell immediately results in the loss of contacts between filaments.

Indeed, any weaving whose ideal configuration contains rectilinear filaments is not dilatant. However, weavings whose ideal forms display curvilinear filaments need not be dilatant. Fig. 5.2 shows the ideal $D_{114C}(3)$ structure, which is a tangled version of the #2 rod packing [OKee 05]. This structure is not dilatant, yet the ideal structure is composed of interwoven helical components. Fig. 5.2 also shows that inflation of the unit cell induces a loss of many inter-filament contacts.

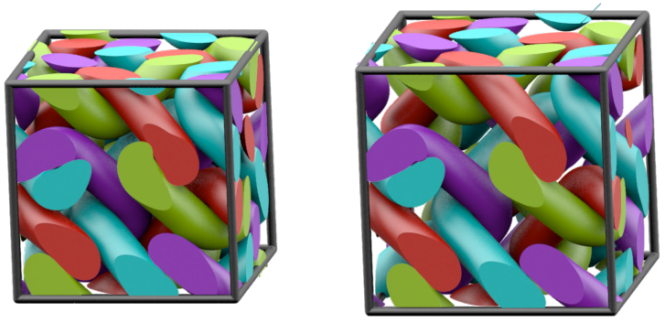

(a) **(b)**

Figure 5.2: The ideal $D_{114C}(3)$ structure, which is a tangled version of the #2 rod packing, is not dilatant. (a) The ideal unit cell, which contains curvilinear fibres. (b) A unit cell inflation induces the loss of some inter-filament contacts *i.e.* the red and blue filaments in the top right corner of the cell are not longer in contact.

Among the 3D weavings generated in Ch. 3, we have found a number of dilatant examples. Recall from the previous chapter, § 4.3.3, the ideal G_{124C} structure (helical Π^+ rod packing) is composed of helical filaments (Fig. 5.3(a)). Successive unit cell expansions

induce straightening of the helical filaments without loss of inter-filament contacts. This expansion can be continued until a final state where the filaments are completely straight and the unit cell is finite, forming the Π^+ rod packing. This is the maximal configuration (Fig. 5.3(b)). The helical filaments of the ideal Π^+ packing have length 6.466 within a $(1 \times 1 \times 1)$ unit cell, and a radius of 0.181: hence the packing fraction is 0.665. On dilation, the packing fraction decreases to 0.295 in the maximal configuration: the packing fraction is more than halved on cooperative straightening.

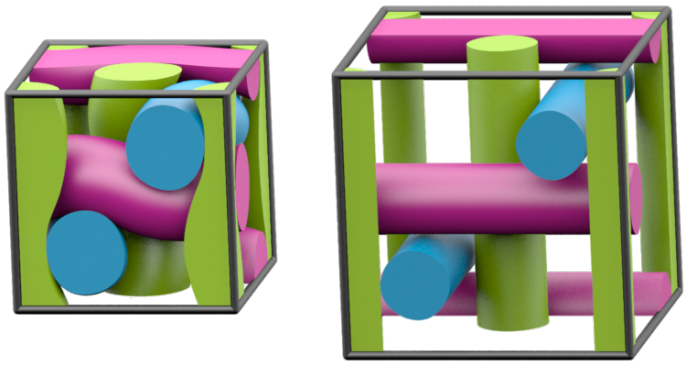

(a) **(b)**

Figure 5.3: The ideal G_{124C} structure (helical Π^+ rod packing) is finitely dilatant. (a) The ideal unit cell. (b) Consecutive unit cell expansions occur without the loss of inter-filament contacts, and the maximal configuration is the Π^+ rod packing.

A particularly large and finite dilatant behaviour is associated with the ideal form of the G_{129C} structure, which is a chiral, cubic arrangement equivalent to a helical Σ^+ rod packing. The ideal structure, shown in Fig. 5.4(a), contains helicoidal filaments that lie almost completely within one channel of the Gyroid surface, as seen in Ch. 4. The maximal configuration of the structure contains straight rods, and is precisely the Σ^+ rod packing (Fig. 5.4(b)). The helical filaments of the ideal structure have length 7.642 within a $(1 \times 1 \times 1)$ unit cell, and a radius of 0.127, and hence a packing fraction of 0.387. The packing fraction of the weaving decreases to 0.075 in the maximal configuration: a 5-fold decrease in the packing fraction. This weaving thus offers a fascinating target structure for rigid weavings capable of extreme variations in filament packing densities.

We also observe finitely dilatant behaviour in anisotropic weavings, such as the trigonal structure $H_{31C}(1)$, constructed in Ch. 3. The ideal structure has undulating filaments in a rhombohedral unit cell, as shown in Fig. 5.5(a). The maximal configuration is a trigonal rod packing of straight components, as shown in Fig. 5.5(b). In the ideal unit cell,

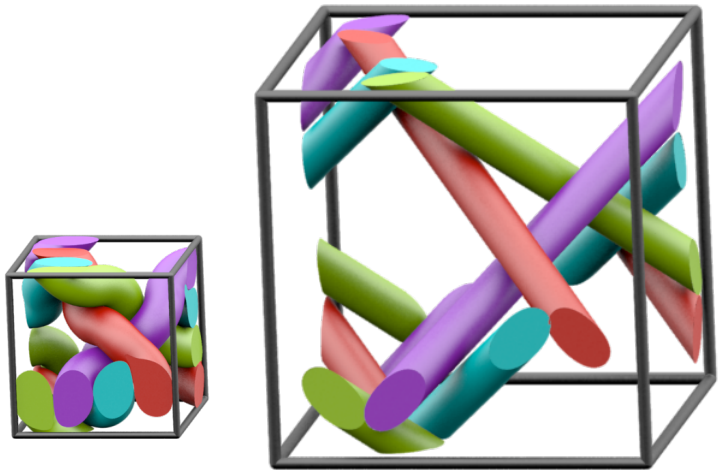

(a) **(b)**

Figure 5.4: The ideal G_{129C} structure, related to the Σ^+ rod packing, is finitely dilatant. (a) The tight unit cell. (b) The maximal state, which has no loss of inter-filament contacts, and is exactly the Σ^+ rod packing.

$L = 4.444$ and $R = 0.181$, which gives a packing fraction of 0.525 (for lattice parameters $(a = b = c = 1;\ \alpha = \beta = \frac{\pi}{2};\ \gamma = \frac{\pi}{3})$). The packing fraction of the weaving decreases to 0.204 in the maximal configuration: more than half of the ideal packing fraction.

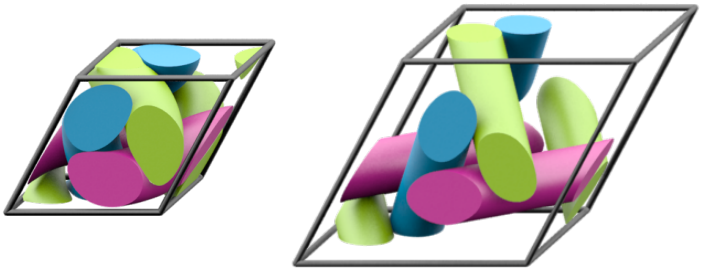

(a) **(b)**

Figure 5.5: The anisotropic trigonal structure $H_{31C}(1)$ is finitely dilatant. (a) The tight unit cell. (b) A unit cell inflation may be performed without the loss of inter-filament contacts, and the maximal configuration is composed of straight rods.

Infinitely dilatant weavings necessarily differ from those weavings that are related to crystallographic rod packings, since in the latter case the (straight) fibres are intersection-free, inducing a maximal configuration with a finite unit cell. However, weavings whose filaments intersect on straightening, as constructed in the previous chapter, § 4.3.3, are infinitely dilatant. In these cases, all inter-filament contacts remain, regardless of the increase in unit cell volume. For example, the weaving $G^{+}_{118C}(1)$, which has intersecting

filaments on straightening and whose ideal configuration is shown in Fig. 5.6(a), is infinitely dilatant. The images in Fig. 5.6(b,c) demonstrate that regardless of the amplitude of a unit cell expansion, all inter-filament contacts remain.

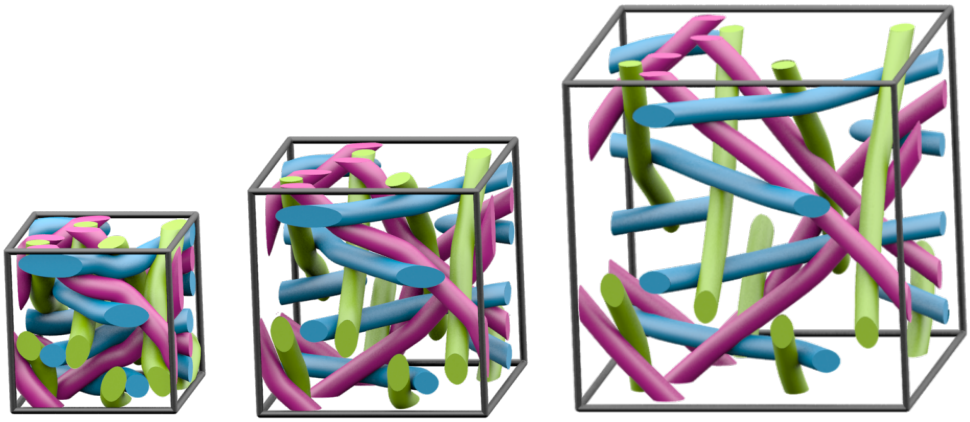

(a) **(b)** **(c)**

Figure 5.6: The ideal $G^{+}_{118C}(1)$ weaving is infinitely dilatant. (a) The ideal unit cell. (b) A small expansion sees all inter-filament contacts remain. (c) A further expansion also sees all contacts preserved. An infinite expansion see all contacts remain and the packing fraction approach zero.

Infinite dilatancy is also seen for the $D_{118C}(1)$ structure, whose ideal and expanded configurations are shown in Fig. 5.7, where all possible unit cell expansions see all inter-filament contacts preserved. It seems, within the limited catalogue of examples constructed in this thesis, that all weavings whose filaments intersect on straightening to their average axes are infinitely dilatant.

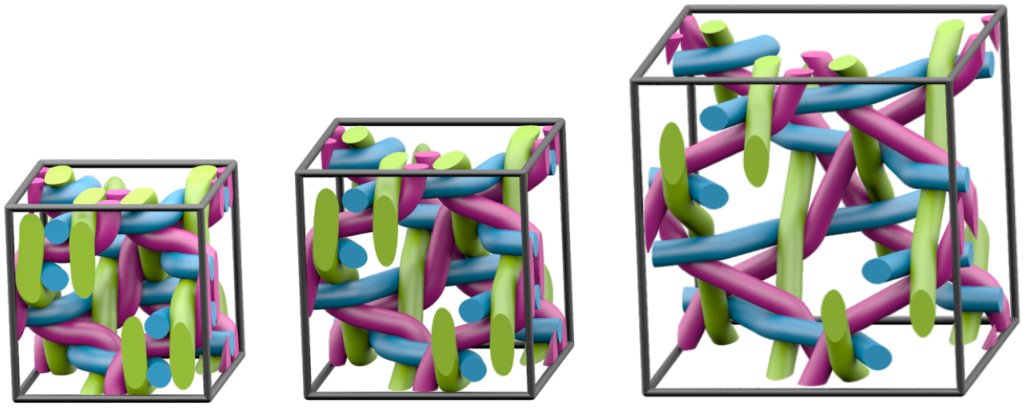

(a) **(b)** **(c)**

Figure 5.7: The $D_{118C}(1)$ structure is infinitely dilatant. (a) The ideal form within one unit cell. (b) A unit cell expansion sees the filaments remain in contact. (c) A further unit cell expansion also has all contacts preserved.

A second genre of infinitely dilatant weaving contains filaments which are sufficiently tangled to preclude rectification of the filaments without changing ambient isotopy type. For example, consider the $G^{+}_{118C}(2)$ structure, which is a tangled version of a packing which contains a triple helix each rod trajectory of the Γ. The unit cell size can be expanded without limit, without the loss of any inter-filament contacts, as illustrated in Fig. 5.8, thus this weaving is infinitely dilatant.

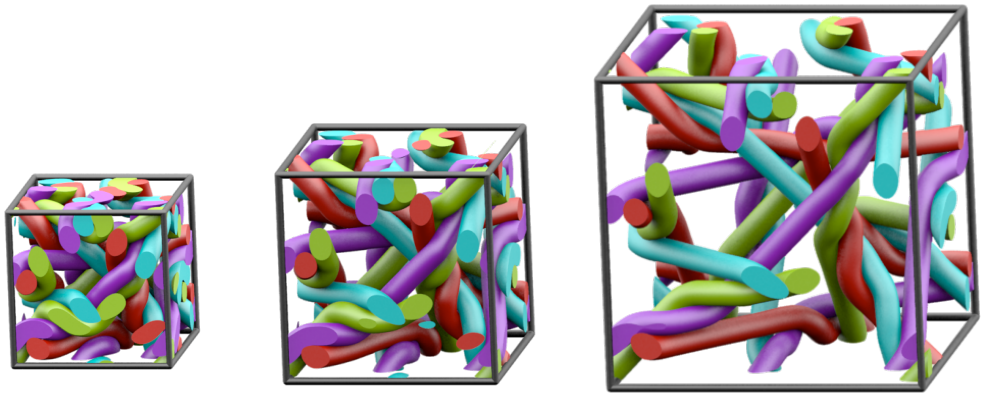

(a) **(b)** **(c)**

Figure 5.8: The ideal $G^{+}_{118C}(2)$ structure is infinitely dilatant. (a) The ideal unit cell. (b) A unit cell expansion sees the filaments remain in contact. (c) A further unit cell expansion also has all contacts preserved.

As a further example, consider the ideal $G^{-}_{118C}(2)$ structure, which is a woven variant of the Σ^{+} rod packing. We see from the consecutive unit cell expansions in Fig. 5.9 that all contacts are preserved through the expansions, and the packing is also infinitely dilatant.

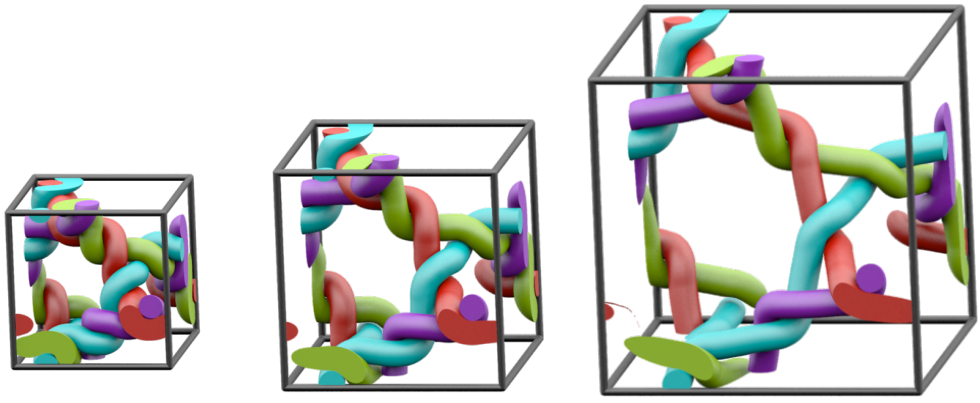

(a) **(b)** **(c)**

Figure 5.9: The ideal $G^{-}_{118C}(2)$ structure, which is a woven Σ^{+} rod packing, is infinitely dilatant. (a) The ideal unit cell. (b) A unit cell expansion sees the filaments remain in contact. (c) A further unit cell expansion also has all contacts preserved.

A formal definition of the rectification transformation for dilatant weavings runs as follows. We construct a one-parameter family of embeddings of weavings parametrised by the variable γ, which describes the fractional dilation. The initial tightest weaving is associated with $\gamma = 0$; the end-state of the dilation process, realised for the maximal configuration is realised when $\gamma = 1$. The magnitude of the dilatancy realised during the expansion process for a variety of weavings is listed in Table 5.1.

Table 5.1: Structural measurements for various structure, all normalised for unit cells of unit volume and fibres of radius R. All weavings are cubic, except $H_{31C}(1)$, which has hexagonal lattice parameters ($a = b = c = 1$; $\alpha = \beta = \frac{\pi}{2}$; $\gamma = \frac{\pi}{3}$). L is the total fibre length per unit cell; γ defines the ideal and maximal states. $f(\gamma)$ denotes the filament volume fraction. The dilatancy induced by fibre rectification is quantified by the fractional change in free and total volumes: Δ_{free} ($= \frac{V_{free}(\gamma_{max})}{V_{free}(0)}$) and Δ_{tot} ($= \frac{V_{tot}(\gamma_{max})}{V_{tot}(0)}$), where V_{free} and V_{tot} denote the free volume and the total unit cell volume respectively.

Structure	**straight?**	**class**	**cubic?**	γ	$R(\gamma)$	$L(\gamma)$	$f(\gamma)$	Δ_{free}	Δ_{tot}
$G^{+}_{123C}(2)$ (Γ)	$\surd$	non-dilatant	cubic	0	0.177	6.933	0.682	1	1
$H_{31C}(1)$	X (ideal)	dilatant (I)	trig.	0	0.181	4.444	0.525		
	$\surd$ (dilated)			1	0.115	4.243	0.204	4.330	2.581
G_{124C}	X (ideal)	”	cubic	0	0.181	6.466	0.662		
(Π^{+})	$\surd$ (dilated)			1	0.125	6	0.295	4.688	2.247
G_{129C}	X (ideal)	”	cubic	0	0.127	7.642	0.384		
(Σ^{+})	$\surd$ (dilated)			1	0.058	6.927	0.073	7.899	5.429
$G^{+}_{118C}(1)$	X (ideal)	dilatant (II)	cubic	0	0.073	18.082	0.303		
	$\surd$ (dilated)			1	0	16.965	0	∞	∞
$D_{118C}(1)$	X (ideal)	”	cubic	0	0.065	19.614	0.260		
	$\surd$ (dilated)			1	0	16.971	0	∞	∞
$G^{-}_{118C}(2)$	X (ideal)	dilatant (III)	cubic	0	0.075	10.714	0.189		
	X (dilated)			< 1	0.03	8.006	0.022	∞	∞
$G^{+}_{118C}(2)$	X (ideal)	”	cubic	0	0.066	29.074	0.398		
	X (dilated)			< 1	0.02	24.284	0.031	∞	∞

We allow only jammed configurations of the weavings during the dilation transformation, for which the number of inter-fibre contacts per unit cell is conserved. Note,

however, that if the fibre length per unit cell is reduced during dilation, the density of inter-fibre contacts per unit cell for outermost fragments of the weaving is reduced, due to this contraction. This variation leads to softening of the weaving rigidity, due to a dearth or excess of unsupported fibres in the corona. This effect is difficult to quantify, due to some flexibility in the fibre arrangement in the (unjammed) corona. A simple gauge is the number of contacts per unit length of the fibre, measured throughout the dilation process. Data are normalised against the G_{124C} weaving, that has the largest number of inter-fibre contacts per unit length of known weavings, whose number of fibre-fibre contacts is scaled to unity.

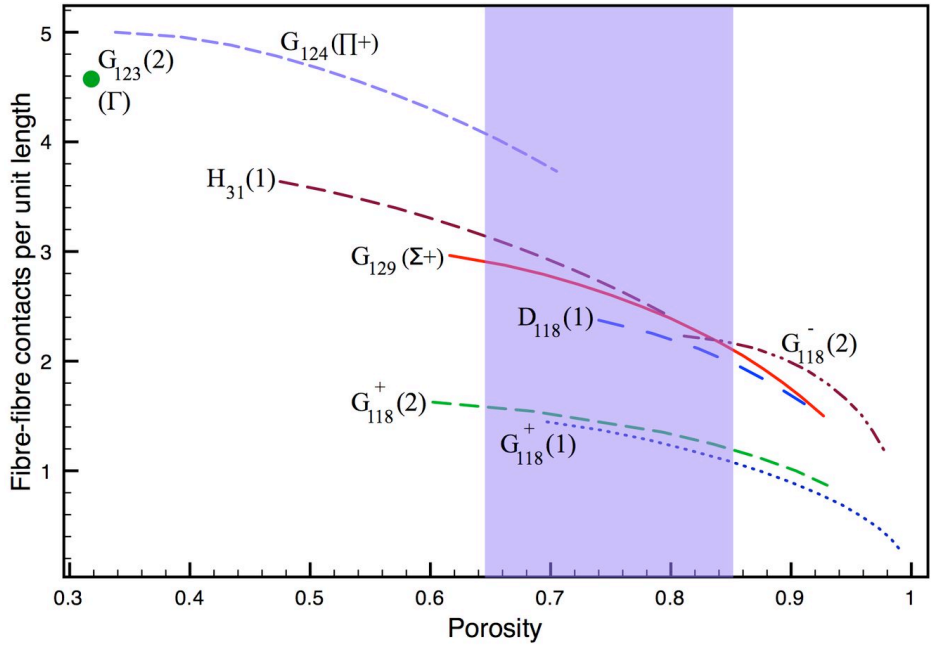

Figure 5.10: Plot of number of inter-filament contacts per unit length (for unit diameter bres) as a function of porosity for a non-dilatant weaving ($G_{123}(2)$) and some finite and infinitely dilatant examples. The shaded region indicates the range of porosities found in human corneocytes from least to most hydrated.

Dilation data for some of the 3D weavings in Table 5.1 are plotted in Fig. 5.10, which allows comparison of the rate of dilation, along with the range of porosities sustained by various weavings. These data reveal the very distinct character of various weavings. Infinitely dilatant weavings exhibit extraordinary dilation properties, however, this is achieved at the expense of significant reduction in the density of inter-fibre contacts. These cases are therefore expected to significantly soften on dilation, and finite volumes of these weavings are likely to unjam on swelling. It is also worth noting that these ex-

amples are less dense (for given porosity) than the finitely dilatant weavings, occupying a significantly larger total volume (for the same total fibre content).

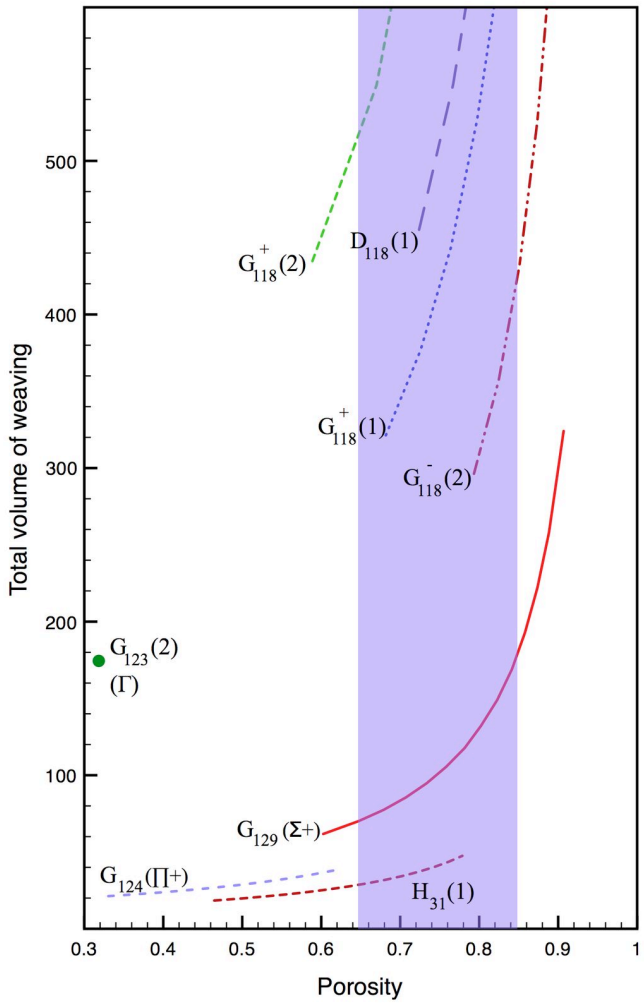

Figure 5.11: Dependence of total weaving volume per unit cell on porosity (where all bres are normalised to unit diameter) for a non-dilatant weaving ($G_{123}(2)$) and some finite and infinitely dilatant examples. The shaded region indicates the range of porosities found in human corneocytes from least to most hydrated.

Among the finitely dilatant weavings, we find significant variation in the material properties as a function of dilation. Two distinct regimes emerge, depending on the porosity of the dilated weavings. If the porosity is less than about 60%, the G_{124C} and $H_{31C}(1)$ weavings are the most compact, with the highest density of inter-fibre contacts. Above this porosity value (to ca. 93%, when the weaving is maximally dilated), dilated versions of the G_{129C} weaving affords the most compact weaving, with the highest density of inter-fibre contacts.

5.2 Keratin alignment in corneocytes

Given the remarkable combination of structural rigidity and variable porosity afforded by the G_{129C} weaving, it is worth looking for traces of the structure in natural materials. One material that necessarily combines these features is mammalian skin. Among its many functions is its homeostatic property on exposure to humidity or water: prolonged immersion in the bath will cause our skin to wrinkle due to swelling, yet this organ retains its structural integrity. The outermost "horny layer" (*stratum corneum*) of mammalian skin is composed of corneocytes, whose interior is dominated by the presence of arrays of helical keratin macrofibres [Brod 59]. On exposure to water, corneocytes can swell to many times their initial volume without significant degradation of the structural integrity of the stratum corneum [Norl 97], due to the uptake of bulk water, which occupies the fibre interstices, thereby reducing the fibre volume fraction [Norl 04]. On hydration, the corneocytes swell with little change in their total fibre content or keratin dimensions, though their helical pitch is likely to vary. In situ measurements of the hydration levels of corneocytes in human *stratum corneum* give average values varying between about 0.5 w/w [Casp 01] and 3 w/w [Bouw 03]. The stratum corneum is predominantly composed of keratin fibres, water and remnant lipids and various water-soluble substances (or 'natural moisturising factors', NMFs), including inorganics, amino acids, proteins and urea [Zhai 89]. Due to the water-binding facility of NMFs, and variation in the NMF contents and hydration within the stratum corneum, estimation of the fraction of keratin fibres within the stratum cornea is difficult to gauge precisely. Assuming densities of 1 gcm^3 for water and NMF and 1.25 gcm^3 for keratin, and a dry mass of about 80% w/w (i.e. NMFs comprise the other 20%) [Ecke 89], the hydration limits reported in [Casp 01, Bouw 03] correspond to keratin volume fractions between 15% and 35%.

The keratin fibres in the stratum corneum therefore form an array whose porosity is capable of varying between 65%-85% without loss of structural rigidity. Comparison of these data with those deduced for dilatant weavings are shown in Fig. 5.10. Evidently, the fibre weaving cannot change types during the hydration process, so a single weaving must span the complete range of porosities. Both the G_{129C} structure (Σ^+) and the $G^+_{118C}(2)$ weavings offer suitable arrangements of keratin fibres with dilatancy squarely within the estimated porosity range. The structure of the soft keratin Intermediate Filaments (IFs) that make up the fibrils as a function of hydration remains uncertain. However, dry fibrils of hard keratins are known to be helical, with pitch 470$\mathring{A}$ and diameter 74.5$\mathring{A}$ [Fras 86],

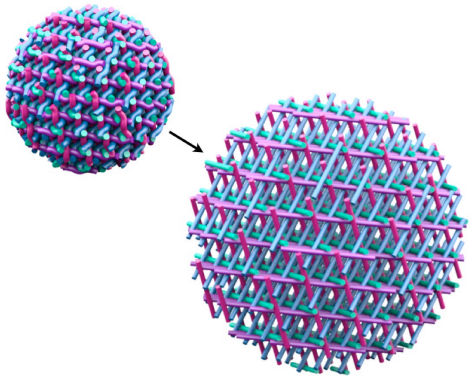

Figure 5.12: Porosity of the material increases as the filaments straighten cooperatively: A spherical section of the G_{129C} material in the tight configuration increases in porosity on straightening of the filaments. The result is the standard configuration of the Σ^+ rod packing.

giving a ratio of pitch to diameter of 6.3. Further, the structure of dry soft keratin IFs, comprising the stratum corneum, is likely to be similar [Fras 86].

The ideal $G^+_{118C}(2)$ weaving contains fibres whose geometry are complex modulated helices, with a simple axis, contrary to the structure of IFs. In contrast, the ideal G_{129C} (Σ^+) weaving is made of helical filaments (which are slightly triangular when projected along their axis, rather than the circular sections of ideal helices). Further, in their tightest configuration, corresponding to the dry state, the ratio of their pitch to fibre diameter is 6.8, close to that proposed by [Fras 86]. (Scaling the (tightest) G_{129C} weaving to give the measured pitch of 470$\mathring{A}$ implies a lattice parameter of about 550$\mathring{A}$ for the weaving.) The remarkable dilatancy of the G_{129C} weaving, which spans the measured porosity variations between dry and hydrated corneocytes, coupled with the agreement in helical dimensions in keratin IFs and the filament shape in the ideal chiral cubic weaving, suggest that keratin fibrils indeed weave within corneocytes according to the G_{129C} pattern. We suggest that the one-parameter family of 3D weavings related to the G_{129C} rod packing best describes the ideal arrangement of keratin fibres within individual corneocytes. Indeed, the G_{129C} rod packing affords a low density, rigid 3D weaving, whose economy makes it an ideal geometry for a biomaterial.

A qualitative picture of the hydration process according to this model runs as follows. Exposure to water induces the keratin fibres to unwind by sliding over each other, without compromising their structural rigidity imposed by their inter-fibre contacts. The number of point contacts per unit cell remains fixed, but they move along the fibres, thereby generating additional free volume accessible to the water. Cooperative unwinding occurs, re-

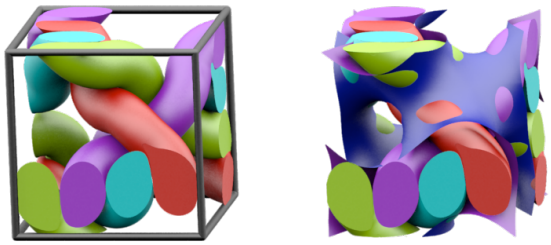

Figure 5.13: The ideal configuration of the G_{129C} structure lies to within a good approximation within a single labyrinth of the gyroid.

sulting in isotropic expansion of the corneocytes. We predict that swelling of corneocytes beyond the free volume accessible to the straightened rod packing will lead to dramatic weakening, since further swelling of the pattern can only occur by losing contacts between fibres, thereby diminishing the structural integrity of the corneocytes. Indeed, there is a limit to water uptake in skin, beyond which the stratum corneum loses its protective barrier [Will 73], (see shaded region in Figs. 5.10 and 5.11).

Evidently this Platonic idealisation of the actual process neglects a number of factors present in the stratum corneum. First, the layer is itself very anisotropic, since it is anchored to the next layer (*stratum lucidum*) on its inner side while its outer face is exposed to the atmosphere; additional structural anisotropy is caused by the pancake-shaped corneocytes. The overall expansion of the layer is therefore unlikely to be isotropic. Secondly, the inter-fibre contacts are probably extended over many atoms; nevertheless, it is likely that in the presence of water keratin fibres slide over each other readily. Finally, since the length per unit cell of fibres changes with swelling, if the total fibre length is conserved – as we expect it is – the total number of inter-fibre contacts diminishes on swelling. The combination of this effect with the changing fibre helicity is expected to induce a measurable variation in the rigidity of corneocytes with hydration, though they remain sterically jammed due to close-packing of the fibres.

It is noteworthy that the G_{129C} weaving is generated by a simple arrangement of geodesics in the gyroid TPMS, a particularly important structure, found in a variety of soft condensed materials, including membrane organelles *in vivo* [Land 95, Alms 06]. Recall also that the ideal configuration lies to within a good approximation within a single labyrinth of the gyroid (see Fig. 5.13). (Indeed, the ideal weaving is sufficiently porous to allow a second ideal weaving of the opposite hand G^{-}_{129C} to be threaded within the G^{+}_{129C}

patttern.) The relation of this weaving with the gyroid is likely more than coincidental. In pioneering structural studies of the *stratum corneum*, Norlén has noted the possible presence of lipid bilayers folded onto the gyroid surface within individual corneocytes and suggested that this geometry effectively templates an ordered arrangement of keratin fibres [Norl 04], corresponding to another weaving whose entanglements are those of the cubic Γ rod packing [OKee 05]. In contrast to the G_{129C} weaving, this pattern is achiral and relatively dense. The Γ embedding is not dilatant, hence the only route to increase the available free volume per unit cell is to lose inter-filament contacts which results in a loss of structural stability. It is noteworthy that despite his discussion of the Γ packing, Norlén suggested a chiral arrangement [Norl 04], consistent with the super-dilatant G_{129C} pattern.

Our model suggests that the corneocytes are formed *in vivo* via templating and collapse to one side of a lipid membrane folded into the gyroid, as proposed by Norlén. The expected lattice parameter for the gyroid, ca. 550$\mathring{A}$, is consistent with dimensions of cubic membranes found to date [Alms 06]. Since Nòrlen's initial proposal, chemical studies have revealed an identical mechanism for the formation of chiral inorganic networks in synthetic mesoporous materials [Ryoo 99, Tera 02]. Most recently, the presence of a chiral, cubic photonic crystal composed of chitin has been established in the wing-scales of certain species of butterflies, leading to structural colour [Mich 08, Sara 10]. Indeed, the chitin network is very similar to the geometry of the keratin fibres, though chitin forms a consolidated network (and resists swelling), in contrast to the individual keratin fibres in the stratum corneum. *Prima facie*, the structural likeness may suggest evolutionary convergence. However, it is most likely that the correspondence of morphology between mammalian skin and butterfly wings is driven by the ubiquity of the gyroid pattern in folded membranes *in vivo*, since both materials are likely templated by a lipid membrane.

Can the extraordinary material properties of mammalian skin be mimicked *in vitro*? Our understanding of the genesis of skin via lipid membrane templating suggests a route to formulate synthetic 3D filament weavings at the macromolecular scale, via templating within bicontinuous molecular mesophases. In addition, the suite of examples of 3D weavings discussed in this paper suggest that this route is a realistic one to generate weavings of various types, from dilatant examples to their conventional counterparts. Evidently, 3D weavings of one-dimensional filaments offer a wealth of distinct material responses as a function of filament geometry.

Chapter 6

Conclusion

In this thesis, we constructed novel, 3-periodic weavings and nets, then tightened them to an "ideal" shape in order to give geometric inspiration to the many disciplines of science influenced by structure. We used a set of Triply-Periodic Minimal Surfaces (TPMS) as a scaffold for their construction. These structures were engineered as tilings of the two dimensional hyperbolic plane ($\mathbb{H}^2$) to harness the simplicity of a two-dimensional surface as compared with 3D space.

To begin, we have developed a catalogue of simple, high symmetry "free" tilings of $\mathbb{H}^2$, which contains examples with both branched tile edges and infinite geodesic tile edges. Furthermore, we have embedded these tilings so as to be candidates for reticulation over the TPMS. For the Stellate orbifolds, we saw that an infinite set of embeddings are possible for a single free tiling, which leads to an infinite set of structures on each of the TPMS. As the embeddings in $\mathbb{H}^2$ become more oblique in shape, the structures that result in $\mathbb{E}^3$ become more entangled in nature.

Further, we constructed an array of 3-periodic structures relevant to the natural sciences. The nets that we constructed are, in most cases, multiple-component interpenetrating nets. Such nets arise frequently in synthetic chemical frameworks [Batt 98, OKee 00], and we generate additional, more complex examples of such nets as possible targets for synthesis. In the construction process, importance is placed on the edge geometry and ambient isotopy class of the net, not simply the topology as is the case for other enumerative techniques. Further, the 3-periodic weavings of filaments constructed in this thesis are, in the simplest cases, well recognised rod packings. Through the TPMS reticulation method, we are able to generalise the notion of a rod packing to contain curvilinear as well as rectilinear fibres, which enables the construction of a more complete taxonomy of 3-periodic weavings. A catalogue of 3-periodic entanglements of infinite filaments is certainly missing from the current literature, and these new structures may provide insight

into weavings of polymers, proteins and DNA.

This thesis has described an extension of the **SONO** algorithm for tightening knots and links: the **PB-SONO** algorithm tightens branched and periodic entanglements. We saw that it performs comparably with the **SONO** algorithm for the tightening of knots. Further, we tightened entangled θ-, tetrahedron- and cube- graphs, which were very accurate for the simplest entanglements (and gave results close to as expected).

We saw "tight" configurations for many periodic nets. The addition of periodicity yielded the uniform embedding as described by the SyStRe algorithm for single component nets. Further, the **PB-SONO** algorithm was able to find a canonical form for nets that have vertex and edge collisions in the SyStRe embedding, as well as a canonical form for non-crystallographic nets. The algorithm handles the interpenetration of multiple component nets in a very intuitive way. The examples shown are convincing evidence that the tight configuration found by the **PB-SONO** algorithm is a very useful tool in analysing geometry and ambient isotopy class of 3-periodic entangled nets, and is applicable to a larger class of structures than have been previously analysed. Evidence of the relevance of the ideal embeddings of nets comes from the ideal structure of two interpenetrating **srs** nets of equivalent chirality, which has equivalent geometry to that given by the crystallographic data for a synthesised framework containing these components. Thus the ideal embedding somehow replicates the conditions within this real chemical framework. The challenge of this method, however, is the numerical error associated with finding these ideal configurations.

An interesting consequence of the idealisation of rod packings to optimal configurations is the geometry of the filaments is helical. Often the geometry prescribed by the idealisation is equivalent to the geometry as the weavings sits on the TPMS, which gives encouragement to the reticulation method of obtaining filament geometry. The helical geometry of some some rod packings in their ideal configurations leads to the exotic physical property of dilatancy.

The consequences of dilatant weavings are immense. These structures are attractive design targets for new synthetic materials, stemming from the potent increases in the free volume of the material on straightening of the filaments, while maintaining structural stability of the material. As a bio-material, this beautiful property in the ideal G_{129C} weaving gives an explanation for the keratin organisation in the corneocytes of the stratum corneum layer of the skin. The dilatancy of the keratin matrix allows us to explain the remarkable structural rigidity of the skin during the uptake of water and subsequent swelling of the

skin. The ramifications of understanding the keratin organisation are immense: the barrier properties of the skin are important in many areas of the medical and therapeutic sciences, and are strongly related to the structural form of the layers within skin.

The scope for further enumeration of more structures of this kind is large. The free tilings of $\mathbb{H}^2$ that have been considered here are a tiny set of the possible tilings of this kind. Firstly, the tiling considered were all of very high symmetry, thus there is scope to extend to lower symmetry groups of $\mathbb{H}^2$. Further, one may consider more oblique embeddings of the free tilings when embedding to be commensurate with the TPMS. We may also generalise further to tilings commensurate with other TPMS of higher genus and also to free tilings which contain both branched boundary components and infinite geodesic boundary components, which will give packings of nets and filaments in unison of the TPMS. In considering only the simplest free tilings on the simplest TPMS, we were able to identify a wealth of interesting structure, and we predict that many more interesting structures will come from further enumeration. We saw that the ideal conformation of a structure often relates to a TPMS reticulation, which gives further encouragement of what we might find on further enumeration of reticulations of these surfaces.

An obvious application of this work is in new materials made from long tangled filaments. For such materials, the dilatancy property discussed may have significant influence in material functionality. Further to this, knowledge of these structures may assist in identifying them in naturally occurring settings, particularly in biological systems. Furthermore, we consider the interesting photonic crystal property of the chitin network in butterfly wings, which is chiral and fills one channel of the gyroid, as described in [Saba 11]. Perhaps a similar effect is present in the chiral keratin arrangement in the skin, which also fills one channel of the gyroid minimal surface. Given a suitable length scale, it may give a partial reflection of the ultra violet spectrum of light, and further act as a natural sunscreen? We saw that many of the 3-periodic weavings displayed both chiral and dilatant properties, which may lead to materials with an interesting fusion of optical and material properties.

Bibliography

[Alms 06] Z. A. Almsherqi, S. D. Kohlwein, and Y. Deng. "Cubic membranes: a legend beyond the flatland of cell membrane organization". *J Cell Biol*, Vol. 173, pp. 839–844, 2006.

[Bage 64] F. Bagemihl. "Analytic continuation and the schwarz reflection principle". *Proc Natl Acad Sci U S A*, Vol. 51, pp. 378–380, 1964.

[Batt 98] S. R. Batten and R. Robson. "Interpenetrating nets: ordered, periodic entanglement". *Angew Chem Int Ed*, Vol. 37, pp. 1460–1494, 1998.

[Bear 95] A. F. Beardon. *The geometry of discrete groups*. Springer-Verlag New York Inc., 1995.

[Blat 06] V. A. Blatov. "Multipurpose crystallochemical analysis with the program package TOPOS". *IUCr CompComm Newsl*, Vol. 7, pp. 4–38, 2006.

[Bouw 03] J. A. Bouwstra, A. de Graaff, G. S. Gooris, J. Nijsse, J. W. Wiechers, and A. C. van Aelst. "Water distribution and related morphology in human stratum corneum at different hydration levels". *J Invest Dermatol*, Vol. 120, pp. 750–758, 2003.

[Brod 59] I. Brody. "The keratinization of epidermal cells of normal guinea pig skin as revealed by electron microscopy". *J Ultrastruc Res*, Vol. 2, pp. 482–511, 1959.

[Buck] G. Buck and J. Simon. "The unified theory of filament entanglement". http://www.gregorybuck.com/pages/pdfs.html.

[Buck 07] G. R. Buck and J. K. Simon. "Total curvature and packing of knots". *Topol Appl*, Vol. 154, pp. 192 – 204, 2007.

[Buck 08] G. Buck, R. G. Scharein, J. Schnick, and J. Simon. "Accessibility and occlusion of biopolymers, ray tracing of radiating tubes, and the temperature of a tangle". *Phys Rev E*, Vol. 77, p. 011803, 2008.

[Buck 93] G. Buck and J. Orloff. "Computing canonical conformations for knots". *Topol Appl*, Vol. 51, pp. 247–253, 1993.

[Buck 95] G. Buck and J. Orloff. "A simple energy function for knots". *Topol Appl*, Vol. 61, pp. 205–214, 1995.

[Buck 98] G. Buck. "Four-thirds power law for knots and links". *Nature*, Vol. 392, pp. 238 – 239, 1998.

[Byrn 08] P. Byrne, G. O. Lloyd, N. Clarke, and J. W. Steed. "A "compartmental" borromean weave coordination polymer exhibiting saturated hydrogen bonding to anions and water cluster inclusion". *Angew Chem*, Vol. 47(31), pp. 5761–5764, 2008.

[Carl 03a] L. Carlucci, G. Ciani, and D. M. Proserpio. "Borromean links and other non-conventional links in polycatenated coordination polymers: re-examination of some puzzling networks". *CrystEngComm*, Vol. 5(47), pp. 269–279, 2003.

[Carl 03b] L. Carlucci, G. Ciani, D. M. Proserpio, and S. Rizzato. "New architectures from the self-assembly of MIISO4 salts with bis(4-pyridyl) ligands. The first case of polycatenation involving three distinct sets of 2D polymeric (4,4)-layers parallel to a common axis". *CrystEngComm*, Vol. 5, pp. 190–199, 2003.

[Carl 03c] L. Carlucci, G. Ciani, and D. M. Proserpio. "Polycatenation, polythreading and polyknotting in coordination network chemistry". *Coord Chem Rev*, Vol. 246, pp. 247 – 289, 2003.

[Carl 99] L. Carlucci, G. Ciani, P. Macchi, D. M. Proserpio, and S. Rizzato. "Complex interwoven polymeric frames from the self-assembly of silver(I) cations and sebaconitrile". *Chem Eur J*, Vol. 5(1), pp. 237–243, 1999.

[Casp 01] P. J. Caspers, G. W. Lucassen, E. A. Carter, H. A. Bruining, and G. J. Puppels. "In vivo confocal raman microspectroscopy of the skin: noninvasive determination of molecular concentration profiles". *J Invest Dermatol*, Vol. 116, pp. 434–442, 2001.

[Cast 08] T. Castle, M. E. Evans, and S. T. Hyde. "Ravels: knot-free but not free. Novel entanglements of graphs in 3-space". *New J Chem*, Vol. 32, pp. 1484–1492, 2008.

[Cast 11a] T. Castle, M. E. Evans, and S. T. Hyde. "Entanglement of embedded graphs". *Prog Theor Phys Supp*, 2011. In press, available at http://people.physics.anu.edu.au/~sth110/Kyoto_tangle_submit_red.pdf.

[Cast 11b] T. Castle, V. Robins, and S. T. Hyde. "Toroidal entangled polyhedral graphs: Tetrahedra, octahedra and cubes". 2011. In preparation.

[Char 85] J. Charvolin. "Crystals of interfaces: the cubic phases of amphiphile/water systems". *J. Phys. Paris*, Vol. 46(C3), pp. 173–190, 1985.

[Chen 01] B. Chen, M. Eddaoudi, S. Hyde, M. O'Keeffe, and O. M. Yaghi. "Interwoven metal-organic framework on a periodic minimal surface with extra-large pores". *Science*, Vol. 291, pp. 1021 – 994, 2001.

[Chun 84] S. J. Chung, T. H. Hahn, and W. E. Klee. "Nomenclature and generation of three-periodic nets: the vector method". *Acta Cryst*, Vol. A40, pp. 42 – 50, 1984.

[Conw 02] J. H. Conway and D. H. Huson. "The orbifold notation for two-dimensional groups". *Struct Chem*, Vol. 13, pp. 247 – 257, August 2002.

[Conw 08] J. H. Conway, H. Burgiel, and C. Goodman-Strauss. "Generalized schläfli symbols". In: *The symmetries of things*, Chap. 20, pp. 269–282, A K Peters Ltd., 2008.

[Conw 67] J. H. Conway. "An enumeration of knots and links, and some of their algebraic properties". In: J. Leech, Ed., *Computation Problems in Abstract Algebra*, pp. 329 – 358, Pergamon Press, Oxford, England, 1967.

[Conw 92] J. Conway. *Groups, combinatorics and geometry*. *London Mathematical Society Lecture Note Series 165*, Cambridge University Press: Cambridge, 1992.

[Coxe 47a] H. S. M. Coxeter. *Non-euclidean geometry*. University of Toronto Press, Toronto, 1947.

[Coxe 47b] H. S. M. Coxeter. *Regular polytopes*. Methuen and Co., 1947.

[Coxe 72] H. S. M. Coxeter and W. O. J. Moser. *Generators and relations for discrete groups*. Springer-Verlag, Berlin, 1972.

[Crom 04] P. Cromwell. *Knots and links*. Cambridge University Press, 2004.

[Delg] O. Delgado-Freidrichs. "Generation, Analysis and Visualization of Reticular Ornaments using GAVROG". available at http://www.gavrog.com.

[Delg 02] O. Delgado-Friedrichs, M. OKeeffe, and O. M. Yaghi. "Three-periodic nets and tilings: regular and quasiregular nets". *Acta Cryst*, Vol. A59, pp. 22–27, 2002.

[Delg 03a] O. Delgado-Friedrichs. "Data structures and algorithms for tilings I". *Theor Comput Sci*, Vol. 303, pp. 431 – 445, 2003.

[Delg 03b] O. Delgado-Friedrichs and M. O'Keeffe. "Identification of and symmetry computation for crystal nets". *Acta Cryst*, Vol. A59, pp. 351 – 361, 2003.

[Dier 92] U. Dierkes, S. Hildebrandt, and F. Sauvigny. *Minimal surfaces*. Vol. 339 of *A series of Comprehensive Studies in Mathematics*, Springer-Verlag, 1992.

[Dioa 98] Y. Dioa, C. Ernst, and E. J. V. Rensburg. "Knots with minimal energies". In: A. Stasiak, V. Katritch, and L. H. Kauffman, Eds., *Ideal Knots*, pp. 52 – 69, World Scientific, 1998.

[Dobr 05] L. Dobrzanska, H. G. Raubenheimer, and L. J. Barbour. "Borromean sheets assembled by self-supporting argentophilic interactions". *Chem Commun*, p. 5050, 2005.

[Doma 05] K. V. Domasevitch, I. Boldog, E. B. Rusanov, J. Hunger, S. Blaurock, M. Schröder, and J. Sieler. "Helical bipyrazole networks conditioned by hydrothermal crystallization". *Z Anorg Allg Chem*, Vol. 631, pp. 1095–1100, 2005.

[Dres 87] A. W. M. Dress. "Presentations of discrete groups, acting on simply connected manifolds, in terms of parametrized systems of Coxeter matrices - a systematic approach". *Adv Math*, Vol. 63, pp. 196 – 212, 1987.

[Ecke 89] R. Eckert. "Structure, function and differentiation of the keratinocyte". *Physiol Rev*, Vol. 69, pp. 1316–1345, 1989.

[Eon 05] J.-G. Eon. "Graph-theoretical characterization of periodicity in crystallographic nets and other infinite graphs". *Acta Cryst*, Vol. A61, pp. 501–511, 2005.

[Eon 11] J.-G. Eon. "Euclidian embeddings of periodic nets: definition of a topologically induced complete set of geometric descriptors for crystal structures". *Acta Cryst*, Vol. A67, pp. 68–86, 2011.

[Fogd 92] A. Fogden and S. T. Hyde. "Parametrisation of triply periodic minimal surfaces. 2. Regular class solutions". *Acta Cryst*, Vol. A48, pp. 575 – 591, 1992.

[Fran 99] G. K. Francis and J. R. Weeks. "Conway's ZIP proof". *Am Math Mon*, Vol. 106, No. 5, pp. 393–399, 1999.

[Fras 86] R. D. Fraser, T. P. MacRae, D. A. Parry, and E. Suzuki. "Intermediate filaments in alpha-keratins". *Proc Natl Acad Sci U S A*, Vol. 83, pp. 1179–1183, 1986.

[Gros 92] J. L. Gross and T. W. Tucker. *Topological graph theory*. Dover Publications, 1992.

[Grze 97] R. P. Grzeszczuk, M. Huang, and L. H. Kauffman. "Physically-based stochastic simplication of mathematical knots". *IEEE T Vis Comput Gr*, Vol. 3(3), pp. 262–272, 1997.

[Hilb 52] D. Hilbert and S. Cohn-Vossen. *Geometry and the imagination*. Chelsea Publishing Group, 1952.

[Huso 93] D. H. Huson. "The generation and classification of tile-k-transitive tilings on the Euclidean plane, sphere, and hyperbolic plane.". *Geometriae Dedicata*, Vol. 47, pp. 295 – 310, 1993.

[Hyde 00a] S. T. Hyde and C. Oguey. "From 2D hyperbolic forests to 3D Euclidean entangled thickets". *Eur Phys J B*, Vol. 16 (2000), pp. 613 – 630, 2000.

[Hyde 00b] S. T. Hyde and S. J. Ramsden. "Chemical frameworks and hyperbolic tilings". In: P. Hansen, P. Fowler, and M. Zheng, Eds., *Discrete Mathematical Chemistry*, pp. 203 – 224, American Mathematical Society, 2000.

[Hyde 00c] S. T. Hyde and S. J. Ramsden. "Polycontinuous morphologies and interwoven helical networks". *Europhys Lett*, Vol. 50, pp. 135 – 141, 2000.

[Hyde 03a] S. T. Hyde, A. K. Larsson, T. D. Matteo, S. J. Ramsden, and V. Robins. "Meditation on an Engraving of Fricke and Klein (The Modular Group and Geometrical Chemistry)". *Aust J Chem.*, Vol. 56, pp. 981 – 1000, 2003.

[Hyde 03b] S. T. Hyde, S. Ramsden, T. D. Matteo, and J. J. Longdell. "Ab-initio construction of some crystalline 3D Euclidean networks". *Solid State Sci*, Vol. 5 (2003), pp. 35 – 45, 2003.

[Hyde 03c] S. T. Hyde and S. J. Ramsden. "Some novel three-dimensional euclidean crystalline networks derived from two-dimensional hyperbolic tilings". *Eur Phys J B*, Vol. 31, pp. 273 – 284, 2003.

[Hyde 06] S. T. Hyde, O. D. Friedrichs, S. J. Ramsden, and V. Robins. "Towards enumeration of crystalline frameworks: the 2D hyperbolic approach". *Solid State Sci*, Vol. 8, pp. 740 – 752, 2006.

[Hyde 07] S. T. Hyde and G. Schröder-Turk. "Tangled (up in) cubes". *Acta Cryst*, Vol. A63, pp. 186–197, 2007.

[Hyde 10] S. T. Hyde, V. Robins, and S. J. Ramsden. "Epinet". http://epinet.anu.edu.au, 2010.

[Hyde 11] S. T. Hyde, S. J. Ramsden, and V. Robins. "A topological approach to two-dimensional crystallography: orbifolds". *in preparation*, 2011.

[Hyde 84] S. T. Hyde and S. Andersson. "A systematic net description of saddle polyhedra and periodic minimal surfaces". *Z Kristallogr*, Vol. 168, pp. 221 – 254, 1984.

[Hyde 91] S. T. Hyde. "Hyperbolic surfaces in the solid-state and the structure of ZSM-5 zeolites". *Acta Chem Scand*, Vol. 45, pp. 860 – 863, 1991.

[Hyde 93] S. T. Hyde. "Crystalline frameworks as hyperbolic films". In: J. Boland and J. D. FitzGerald, Eds., *Defects and processes in the solid state: Geoscience applications*, Elsevier, Amsterdam, 1993.

[Hyde 97] S. T. Hyde, S. Andersson, K. Larsson, Z. Blum, T. Landh, S. Lidin, and B. W. Ninham. *The language of shape: the role of curvature in condensed matter: physics, chemistry and biology*. Elsevier Science B.V., 1997.

[Hyde 99] S. T. Hyde and S. J. Ramsden. "Crystals. Two-dimensional non-euclidean geometry and topology". In: D. Bonchev and D. Rouvray, Eds., *Chemical Topology: Applications and Techniques*, pp. 35 – 174, Gordon and Breach Science Publishers, N.Y., 1999.

[Jang 09] J.-J. Jang, L. Li, T. Yang, D.-B. Kuang, W. Wang, and C.-Y. Su. "Self-assembly of 2D borromean networks through hydrogen-bonding recognition". *Chem Commun*, pp. 2387–2389, 2009.

[Kabl 07] A. Kabla and L. Mahadevan. "Nonlinear mechanics of soft fibre networks". *J. R. Soc. Interface*, Vol. 4(12), pp. 99–106, 2007.

[Katr 96] V. Katritch, J. Bednar, D. Michoud, R. G. Scharein, J. Dubochet, and A. Stasiak. "Geometry and physics of knots". *Nature*, Vol. 384, pp. 142–145, 1996.

[Kepe 00] C. J. Kepert, T. J. Prior, and M. J. Rosseinsky. "A versatile family of interconvertible microporous chiral molecular frameworks: the first example of ligand control of network chirality". *J Am Chem Soc*, Vol. 122, pp. 5158–5168, 2000.

[Kepe 98] C. J. Kepert and M. J. Rosseinsky. "A porous chiral framework of coordinated 1,3,5–benzenetricarboxylate: quadruple interpenetration of the (10,3)-a network". *Chem Commun*, pp. 31–32, 1998.

[Kirk 84] S. Kirkpatrick, C. D. Gelatt, and M. P. Vecchi. "Optimization by simulated annealing". *Science*, Vol. 220, pp. 671–680, 1984.

[Klee 04] W. Klee. "Crystallographic nets and their quotient graphs". *Cryst Res Technol*, Vol. 39, pp. 959–968, 2004.

[Koch 99] E. Koch and W. Fischer. "Sphere packings and packings of ellipsoids". In: *International Tables for Crystallography, Vol. C (Second revised edition)*, pp. 738 – 743, Kluwer Academic Publishers, 1999.

[Kusn 97] R. B. Kusner and J. M. Sullivan. *Geometric Topology*. AMS/International Press, Cambridge, MA, 1997.

[Land 95] T. Landh. "From entangled membranes to eclectic morphologies – cubic membranes as subcellular space Organisers". *FEBS Lett*, Vol. 369(1), pp. 13–17, 1995.

[Laur 98] B. Laurie. "Annealing ideal knots and links: methods and pitfalls". In: A. Stasiak, V. Katritch, and L. H. Kauffman, Eds., *Ideal Knots*, pp. 42 – 51, World Scientific, 1998.

[Lezn 01] D. B. Leznoff, B.-Y. Xue, R. J. Batchelor, F. W. B. Einstein, and B. O. Patrick. "Gold/gold interactions as crystal engineering design elements in heterobimetallic coordination polymers". *Inorg Chem*, Vol. 40(23), p. 60266034, 2001.

[Li 07] J. Li, L. Song, and S. Du. "A novel borromean (6, 3) net assembled by nest-shaped clusters WOS3Cu3 as knots". *Inorg Chem Commun*, Vol. 10(3), pp. 358–361, 2007.

[Li 11] F. Li, J. K. Clegg, L. F. Lindoy, R. B. Macquart, and G. V. Meehan. "Metallosupramolecular Self-Assembly of a Universal 3-Ravel". *Nat Commun*, 2011. In press.

[Lian 03] R. Liantonio, P. Metrangolo, T. Pilati, and G. Resnati. "Fluorous interpenetrated layers in a three-component crystal matrix". *Cryst Growth Des*, Vol. 3(3), p. 355361, 2003.

[Lian 06] R. Liantonio, P. Metrangolo, F. Meyer, T. Pilati, W. Navarrini, and G. Resnati. "Metric engineering of supramolecular Borromean rings". *Chem Commun*, p. 1819, 2006.

[Lord 06] E. A. Lord, A. L. Mackay, and S. Ranganthan. *New geometries for new materials*. Cambridge University Press, 2006.

[Lu 06] X.-Q. Lu, M. Pan, J.-R. He, Y.-P. Cai, B.-S. Kang, and C.-Y. Su. "Three-fold parallel interlocking of 2-D brick-wall networks showing ladder-like unsymmetrical borromean links". *CrystEngComm*, Vol. 8(8), p. 827, 2006.

[Mari 00] A. Maritan, C. Micheletti, A. Trovato, and J. Banavar. "Optimal shapes of compact strings". *Nature*, Vol. 406, pp. 287 – 288, 2000.

[Men 09] Y.-B. Men, J. Sun, Z.-T. Huang, and Q.-Y. Zheng. "Rational construction of 2D and 3D borromean arrayed organic crystals by hydrogen-bond-directed self-assembly". *Angew Chem*, Vol. 48(16), pp. 2873–2876, 2009.

[Mich 08] K. Michielsen and D. G. Stavenga. "Gyroid cuticular structures in butterfly wing scales: biological photonic crystals". *J. R. Soc. Interface*, Vol. 5, pp. 85–94, 2008.

[Moln 02] E. Molnar. "On triply periodic minimal balance surfaces". *Struct Chem*, Vol. 13, pp. 267–275, 2002.

[Mori 04] H. Moriuchi. "An enumeration of theta-curves with up to seven crossings, Proceedings of the East Asian School of Knots, Links and Related Topics". 2004. Available at knot.kaist.ac.kr/2004/proceedings.php.

[Muth 02] S. Muthu, J. H. K. Yip, and J. J. Vittal. "Coordination networks of Ag(I) and N,N- bis(3-pyridinecarboxamide)-1,6-hexane: structures and anion exchange". *J Chem Soc, Dalton Trans*, p. 4561, 2002.

[Norl 04] L. Norlén and A. Al-Amoudi. "Stratum corneum keratin structure, function, and formation: the cubic rod-packing and membrane Templating Model". *J Invest Dermatol*, Vol. 123, pp. 715–732, 2004.

[Norl 97] L. Norlén, A. Emilson, and B. Forslind. "Stratum corneum swelling. Biophysical and computer assisted quantitative assessments". *Arch Dermatol Res*, Vol. 289, pp. 506–513, 1997.

[OKee 00] M. O'Keeffe, M. Eddaoudi, H. Li, T. Reineke, and O. M. Yaghi. "Frameworks for extended solids: geometry design principles". *J Solid State Chem*, Vol. 152, pp. 3–20, 2000.

[OKee 01] M. O'Keeffe, J. Plevert, Y. Teshima, Y. Watanabe, and T. Ogama. "The invariant cubic rod (cylinder) packings: symmetries and coordinates". *Acta Cryst*, Vol. A57, pp. 110–111, 2001.

[OKee 05] M. O'Keeffe. "Rod packings and metal-organic frameworks constructed from rod-shaped secondary building units". *J Amer Chem Soc*, Vol. 127(5), pp. 1504–1518, 2005.

[OKee 08] M. O'Keeffe, M. A. Peskov, S. J. Ramsden, and O. Yaghi. "The reticular chemistry structure resource (RCSR) database of, and symbols for, crystal Nets". *Accts Chem Res*, Vol. 41, pp. 1782–1789, 2008.

[OKee 96] M. O'Keeffe and B. G. Hyde. *Crystal structures I. Patterns and symmetry*. Mineralogical Society of America, 1996.

[Olse 10] K. Olsen and J. Bohr. "The generic geometry of helices and their close-packed structure". *Theor Chem Acc*, Vol. 125, pp. 207 – 215, 2010.

[OHa 91] J. OHara. "Energy of a knot". *Topology*, Vol. 30(2), pp. 241–247, 1991.

[Pier 98] P. Pieranski. "In search of ideal knots". In: A. Stasiak, V. Katritch, and L. H. Kauffman, Eds., *Ideal Knots*, pp. 20 – 41, World Scientific, 1998.

[Przy 01] S. Przybyl and P. Pieranski. "Helical close packing of ideal ropes". *Eur Phys J E*, Vol. 4(4), pp. 445 – 449, 2001.

[Rams 09] S. J. Ramsden, V. Robins, and S. T. Hyde. "Three-dimensional euclidean nets from two-dimensional hyperbolic tilings: kaleidoscopic examples". *Acta Cryst*, Vol. A65, pp. 81–108, 2009.

[Robi 04a] V. Robins, S. J. Ramsden, and S. T. Hyde. "2D hyperbolic groups induce three-periodic euclidean reticulations". *Eur Phys J B*, Vol. 39, pp. 365 – 375, 2004.

[Robi 04b] V. Robins, S. J. Ramsden, and S. T. Hyde. "Symmetry groups and reticulations of the hexagonal H surface". *Physica A*, Vol. 339, pp. 173–180, 2004.

[Robi 05] V. Robins, S. J. Ramsden, and S. T. Hyde. "A note on the two symmetry-preserving covering maps of the gyroid minimal surface". *Eur Phys J B*, Vol. 48, pp. 107–111, 2005.

[Ryoo 99] R. Ryoo, S. H. Joo, and S. Jun. "Synthesis of highly ordered carbon molecular sieves via template–mediated structural transformation". *J Phys Chem B*, Vol. 103, p. 7743, 1999.

[Saba 11] M. Saba, M. Thiel, M. D. Turner, S. Hyde, M. Gu, K. Grosse-Brauckmann, D. N. Neshev, K. Mecke, and G. E. Schröder-Turk. "Circular dichroism in biological photonic crystals and cubic chiral nets". *Phys Rev Lett*, 2011. in press.

[Sado 89] J. F. Sadoc and J. Charvolin. "Infinite periodic minimal surfaces and their crystallography in the hyperbolic plane". *Acta Cryst*, Vol. A45, pp. 10 – 20, 1989.

[Sado 90] J. F. Sadoc. *Geometry in condensed matter physics*. Vol. 9 of *Directions in condensed matter physics*, World Scientific, 1990.

[Sara 10] V. Saranathan, C. O. Osuji, S. G. J. Mochrie, H. Noh, S. Narayanan, A. Sandy, E. R. Dufresne, and R. O. Prum. "Structure, function, and self-assembly of single network gyroid ($I4_132$) photonic crystals in butterfly wing scales". *Proc Natl Acad Sci U S A*, Vol. 107(26), pp. 11676–11681, 2010.

[Scha 98] R. G. Scharein. *Interactive topological drawing*. PhD thesis, Department of Computer Science, The University of British Columbia, 1998.

[Scho 70] A. H. Schoen. "Infinite periodic minimal surfaces without self-intersections". *NASA Technical Note*, Vol. TN D-5541, 1970.

[Shar 00] C. V. K. Sharma, R. J. Diaz, A. J. Hessheimer, and A. Clearfield. "Double stranded chains and interwoven structures: the role of conformational isomerism in coordination polymers". *Cryst Eng*, Vol. 3(3), pp. 201–208, 2000.

[Simo 09] J. Simon. "Long tangled filaments". In: D. Buck and E. Flapan, Eds., *Applications of knot theory*, pp. 155 – 181, American Mathematical Society, 2009.

[Simo 94] J. K. Simon. "Energy functions for polygonal knots". *J Knot Theor Ramif*, Vol. 3(3), pp. 299–320, 1994.

[Spiv 79] M. Spivak. *A comprehensive introduction to differential geometry*. Vol. 5, Publish or Perish Inc., 1979.

[Stas 98] A. Stasiak, J. Dubochet, V. Katritch, and P. Pieranski. "Ideal knots and their relation to the physics of real knots". In: A. Stasiak, V. Katritch, and L. H. Kauffman, Eds., *Ideal Knots*, pp. 1 – 19, World Scientific, 1998.

[Stil 87] J. Stillwell. *Geometry of surfaces*. Springer-Verlag, 1987.

[Suh 03] M. P. Suh, H. J. Choi, S. M. So, and B. M. Kim. "A new metal-organic open framework consisting of threefold parallel interwoven (6,3) nets". *Inorg Chem*, Vol. 42(3), p. 676678, 2003.

[Tera 02] O. Terasaki, Z. Liu, T. Ohsuna, H. J. Shin, and R. Ryoo. "Electron microscopy study of novel Pt nanowires synthesized in the spaces of silica mesoporous materials". *Microsc Microanal*, Vol. 8, pp. 35–39, 2002.

[Thur 80] W. Thurston. *The geometry and topology of three-manifolds*. Princeton University: Princeton, New Jersey, 1980.

[Tong 99] M.-L. Tong, X.-M. Chen, B.-H. Ye, and L.-N. Ji. "Self-assembled three-dimensional coordination polymers with unusual ligand-unsupported Ag-Ag bonds: syntheses, structures, and luminescent properties". *Angew Chem*, Vol. 38(15), pp. 2237–2240, 1999.

[Well 77] A. E. Wells. *Three-dimensional nets and polyhedra*. *Wiley monographs in crystallography*, Wiley-Interscience, 1977.

[Will 73] I. Willis. "The effects of prolonged water exposure on human skin". *J Invest Dermatol*, Vol. 60, pp. 166 – 171, 1973.

[Zhai 89] H. Zhai, H. I. Maibach, and K.-P. Wilhelm, Eds. *Dermatotoxicology*. Informa Healthcare, seventh Ed., 1989.

[Zhan 07a] X.-L. Zhang, C.-P. Guo, Q.-Y. Yang, T.-B. Lu, Y.-X. Tong, and C.-Y. Su. "Discrete chiral single-crystal microtubes assembled with honeycomb coordination networks showing structural diversity and borromean topology in one single crystal". *Chem Mater*, Vol. 19, p. 4630, 2007.

[Zhan 07b] X.-L. Zhang, C.-P. Guo, Q.-Y. Yang, W. Wang, W.-S. Liu, B.-S. Kang, and C.-Y. Su. "Formation of two (6,3) networks showing structural diversity, borromean topology and conformational chirality in the same crystal". *Chem Commun*, p. 42424244, 2007.

Appendix A

Commensurate orbifold subgroups

Table A.1: Subgroups of $*246$ commensurate with the P, D and G minimal surfaces [Robi 04a].

Group #	Orbifold	Index	Maximal subgroups
131	$*246$	1	130, 129, 128, 127, 126 125, 124, 123, 122
130	246	2	120, 118, 116, 114, 93
129	$2*23$	2	121, 119, 118, 113, 99
128	$4*3$	2	121, 117, 116, 110, 98
127	$*266$	2	120, 119, 117, 104, 96
126	$6*2$	2	121, 120, 115, 100, 94
125	$*344$	2	119, 116, 115, 107, 95
124	$*2223$	2	118, 117, 115, 102, 97
123	$*2224$	3	114, 113, 112, 111, 110, 109, 108, 107, 106, 105, 104, 103, 102, 101, 100
122	$2*26$	4	99, 98, 97, 96, 95, 94, 93, 89
121	$23\times$	4	92, 53, 52
120	266	4	92, 54, 50
119	$*2323$	4	92, 81, 48
118	2223	4	92, 49, 77
117	$2*33$	4	92, 65, 47
116	344	4	92, 86, 51
115	$3*22$	4	92, 55, 46
114	2224	6	87, 86, 78, 77, 76, 61, 54
113	$2*22$	6	81, 80, 79, 77, 75, 56, 53
112	$**2$	6	85, 82, 80, 73, 72, 70, 61
111	$22*2$	6	85, 79, 76, 68, 67, 66, 58
110	$24*$	6	86, 85, 84, 65, 62, 59, 53
109	$24*$	6	87, 84, 74, 73, 71, 58, 56
108	$2*44$	6	84, 82, 78, 75, 69, 66, 64
107	$*2244$	6	86, 81, 74, 70, 68, 64, 55

Table A.1: Subgroups of $*246$ commensurate with the P, D and G minimal surfaces [Robi 04a].

Group #	Orbifold	Index	Maximal subgroups
106	$4*22$	6	79, 78, 74, 72, 63, 62, 57
105	$**2$	6	69, 68, 63, 61, 60, 59, 56
104	$2*222$	6	83, 82, 81, 65, 63, 58, 54
103	$*2244$	6	87, 83, 80, 67, 64, 62, 60
102	$*22222$	6	77, 73, 66, 65, 60, 57, 55
101	$*22222$	6	91, 90, 89, 88, 83, 76, 75, 71, 70, 59, 57
100	$2*222$	6	72, 71, 69, 67, 55, 54, 53
99	$22*3$	8	52, 49, 48, 42
98	$*3\times$	8	52, 51, 47, 40
97	$22*3$	8	49, 47, 46, 37
96	$*2626$	8	50, 48, 47, 36
95	$*3\times$	8	51, 48, 46, 45
94	$26\times$	8	52, 50, 46, 15
93	2226	8	51, 50, 49, 44
92	2323	8	14, 13
91	$*22*$	12	43, 42, 40, 39, 38, 34, 30
90	$2*2222$	12	44, 39, 36, 35, 34, 33, 23
89	$22*22$	12	45, 44, 42, 40, 37, 36, 15
88	$2**$	12	45, 43, 38, 37, 35, 33, 31
87	2244	12	27, 18, 17
86	2244	12	21, 17, 14
85	$2\times\times$	12	29, 21, 19
84	$44\times$	12	32, 19, 17
83	$*222222$	12	38, 36, 28, 27, 20
82	$*22\times$	12	28, 24, 19
81	$22*22$	12	28, 26, 14
80	$*2*2$	12	29, 28, 18
79	$222\times$	12	29, 26, 16
78	2244	12	24, 17, 16
77	22222	12	18, 16, 14
76	22222	12	44, 43, 27, 21, 16
75	$22*22$	12	42, 35, 32, 28, 16
74	$44*$	12	26, 22, 17
73	$2**$	12	22, 19, 18
72	$2*\times$	12	41, 31, 29, 24, 22
71	$222*$	12	32, 31, 30, 27, 23, 22, 15
70	$**22$	12	45, 39, 28, 22, 21
69	$*22\times$	12	41, 32, 30, 25, 24
68	$*2*2$	12	26, 25, 21
67	$22*22$	12	41, 29, 27, 25, 23
66	$22*22$	12	25, 19, 16
65	$222*$	12	20, 19, 14

Table A.1: Subgroups of $*246$ commensurate with the P, D and G minimal surfaces [Robi 04a].

Group #	Orbifold	Index	Maximal subgroups
64	$*4444$	12	28, 25, 17
63	$2*\times$	12	26, 24, 20
62	$44*$	12	29, 20 17
61	$\circ 2$	12	24, 21, 18
60	$**22$	12	25, 20, 18
59	$2**$	12	40, 33, 32, 21, 20
58	$222\times$	12	27, 26, 19
57	$2*2222$	12	37, 34, 22, 20, 16
56	$2\times\times$	12	32, 26, 18
55	$*222222$	12	25, 22, 14
54	22222	12	27, 24, 14
53	$222\times$	12	32, 29, 14
52	$3\times\times$	16	13, 4
51	$\circ 3$	16	13, 12
50	2266	16	13, 2
49	22223	16	13, 11
48	$*3*3$	16	13, 10
47	$*3*3$	16	13, 9
46	$3\times\times$	16	13, 3
45	$*\times\times$	24	12, 10, 3
44	222222	24	12, 11, 2
43	$\circ 22$	24	12, 11, 8
42	$22*\times$	24	11, 10, 4
41	$*\times\times$	24	8, 6, 5
40	$*\times\times$	24	12, 9, 4
39	$**\times$	24	12, 10, 6
38	$***$	24	10, 9, 8
37	$22*\times$	24	11, 9, 3
36	$22*2222$	24	10, 9, 2
35	$22*\times$	24	11, 10, 5
34	$*2222\times$	24	11, 9, 6
33	$**\times$	24	12, 9, 5
32	$22\times\times$	24	7, 5, 4
31	$\times\times\times$	24	8, 5, 3
30	$\circ*$	24	8, 6, 4
29	$22\times\times$	24	7, 5
28	$*22*22$	24	10, 7
27	222222	24	8, 7, 2
26	$22\times\times$	24	7
25	$*22*22$	24	7, 6
24	$\circ 22$	24	8, 7
23	$2222*$	24	6, 5, 2

Table A.1: Subgroups of $*246$ commensurate with the P, D and G minimal surfaces [Robi 04a].

Group #	Orbifold	Index	Maximal subgroups
22	$22**$	24	7, 6, 3
21	$\circ 22$	24	12, 7
20	$22**$	24	9, 7
19	$22\times\times$	24	7
18	$\circ 22$	24	7
17	4444	24	7
16	222222	24	11, 7
15	$2222\times$	24	4, 3, 2
14	222222	24	7
13	$\circ 33$	32	1
12	$\circ\circ$	48	1
11	$\circ 2222$	48	1
10	$****$	48	1
9	$****$	48	1
8	$\circ\circ$	48	1
7	$\circ 2222$	48	1
6	$\circ**$	48	1
5	$\times\times\times\times$	48	1
4	$\times\times\times\times$	48	1
3	$\times\times\times\times$	48	1
2	22222222	48	1
1	$\circ\circ\circ$	96	

Table A.2: Subgroups of $*2226$ commensurate with the H minimal surface [Robi 04b].

Group #	Orbifold	Index
32	$*2226$	1
31	2226	2
30	$26*$	2
29	$22*3$	2
28	$*3*$	2
27	$*3*$	2
26	$*22223$	2
25	$*2266$	2
24	$2*2222$	3
23	2626	4
22	22223	4
21	$3\times\times$	4
20	$\circ 3$	4
19	$*33*$	4
18	$3**$	4
17	$*3*3$	4
16	$22*\times$	6
15	222222	6
14	$*2222\times$	6
13	$**\times$	6
12	$**\times$	6
11	$22*2222$	6
10	$2222*$	6
9	$\circ 33$	8
8	$**\times\times$	12
7	$\circ 2222$	12
6	$\circ\circ$	12
5	$**\times\times$	12
4	$\times\times\times\times$	12
3	$\circ**$	12
2	22222222	12
1	$\circ\circ\circ$	24